JOURNAL OF SOLID STATE CHEMISTRY 115, 525–531 (1995)

Synthesis and Characterization of Mercury-Based "1222" Cuprates $(Hg_{1-x}M_x)(Sr,Ba)_2Pr_2Cu_2O_{9-\delta}$ (M = Pr, Pb, Bi, Tl)

M. Hervieu, G. Van Tendeloo,* C. Michel, C. Martin, A. Maignan, and B. Raveau

*Laboratoire CRISMAT-ISMRA et Université de Caen Boulevard du Maréchal Juin, 14050 Caen Cedex, France; and *RUCA, University of Antwerp, Groenenborgerlaan 171, B 2020 Antwerp, Belgium*

Received May 5, 1994; in revised form July 27, 1994; accepted July 28, 1994

Five new layered cuprates, with a 1222-type structure, have been synthesized according to the formula $(Hg_{1-x}M_x)(Sr,Ba)_2Pr_2Cu_2O_{9-\delta}$ with M = Pr, Pb, Bi, and Tl. They crystallize in a tetragonal cell with $a \approx a_p$ and $c \approx 29.5$ Å; their structure consists *in a triple intergrowth of oxygen-deficient perovskite, rock-salt-* and fluorite-type layers. They are characterized by a mixed $[Hg_{1-x}M_xO_{1-\delta}]$ layer in the rock-salt-type slice. The ED and HREM studies show that Tl, Bi, and Pb are statistically distributed in the mixed $[Hg_{1-x}M_xO_{1-\delta}]$ layer, contrary to Pr which involves an ordering phenomenon along a. Different stacking defects are observed and discussed as well as the cleavage mode of the crystals.

INTRODUCTION

The studies carried out these past 8 years on the research of new layered copper oxides have shown the great ability of three structural types, perovskite, rock-salt, and fluorite, to accommodate each other so that numerous intergrowths of these three structures can be generated (for an overview, see Ref. 1). Especially, the Jahn–Teller effect of copper that leads to the formation of layers of CuO_5 pyramids causes the alkaline earth or rare earth cations intercalculated between these sheets to form single fluorite-type layers. As a result it has been shown that additional $[Ln_2O_2]_\infty$ layers can be intercalated between the copper layers, either in the form of extended defects (2) or as regular structures (3–7). Starting from the single fluorite-type cuprates, denoted "n212," that exhibit single (n = 0), double (n = 1), or triple (n = 2) rock-salt-type layers, double fluorite cuprates "n222" have been generated (3, 4, 8). The study of these oxides is of interest for the structural aspects of superconductivity at high temperature. One indeed observes that contrary to the "n212" oxides that are high T_c superconductors, most of the "n222" cuprates exhibit a semiconducting behavior or superconductivity with a very low diamagnetic fraction.

In the 1222 oxides, it was shown that the intermediate $[AO]$ layer can be stabilized with thallium and/or lead atoms [3, 6, 7, 9). The recent discovery of the mercury-based "1212" superconductors, exhibiting either a $[HgO_{1-\delta}]$ (10) layer or a mixed $[Hg_{1-x}MxO_{1-\delta}]$ layer with M = Pb (11), Bi (12), and Pr (13), suggests the possibility of isolating isotypic mercury-based 1222 cuprates. This paper deals with the characterization of a new series of oxides, corresponding to the general formula $(Hg_{1-x}M_x)(Ba,Sr)_2Pr_2Cu_2O_{9-\delta}$.

EXPERIMENTAL

The different compositions of the systems $(Hg_{1-x}M_x)(Sr_{2-y}Ba_y)Pr_2Cu_2O_{9-\delta}$, with M = Pb, Bi, Tl, Pr, were investigated from the adequate mixtures of the oxides HgO, PbO, Bi_2O_3, Tl_2O_3, Pr_6O_{11}, BaO_2, CuO, SrO_2, and Sr_2CuO_3. They were sealed in silica tubes and heated at 800°C for 12 hr. The phase purity of the products was systematically checked by X-ray diffraction (XRD) and electron diffraction (ED); the compositions were analyzed by energy dispersive X-ray spectroscopy (EDS); the analyses have been carried out, taking as standards several binary and ternary oxides of the different systems such as $HgSrO_2$, $BaPrO_3$, Sr_2CuO_3, $Tl_2Ba_2CuO_6$, $SrPbO_3$, $Ba_2Bi_6O_{11}$, and $Tl_{0.5}Pb_{0.5}Sr_2CaCu_2O_{7-\delta}$.

The as-synthesized samples were annealed in oxygen at pressures up to 100 bar at 720 K or in an argon flow.

XRD patterns were registered using a Philips vertical diffractometer (Cu$K\alpha$ radiation). Data were collected in the range $10° \leq 2\theta \leq 80°$ by step scanning with an increment of 0.02° (2θ). Lattice constants and crystal structure were refined using the Rietveld method (computer program DBW 3.2 (14)).

The ED study was performed with a JEOL 200CX electron microscope fitted with a side entry goniometer (±60°); high resolution electron microscopy was carried out with a TOPCON 002B microscope, having a 1.8 Å point resolution.

Electrical resistance measurements were performed by a standard four-probe method operating in dc mode, with

0022-4596/95 $6.00

currents ranging from 10^{-6} to 10^{-3} A, and the temperature was swept from 4.2 K to room temperature.

Magnetic measurements were carried out with a SQUID magnetometer at 5 K.

RESULTS AND DISCUSSION

According to the above thermal process, the different systems have been investigated, for $0.3 \leq x \leq 1$ and $0 \leq y \leq 1$. The XRD patterns show the existence of a "1222"-type phase for most of the nominal compositions; however, EDS analyses performed on numerous grains of the different samples evidence very small existence domains: in that way, the homogeneity range is practically limited to one composition in the case of thallium, lead, and bismuth compounds, i.e., $Hg_{0.3}Tl_{0.7}Sr_2Pr_2Cu_2O_{9-\delta}$, $Hg_{0.3}Pb_{0.7}Sr_2Pr_2Cu_2O_{9-\delta}$, and $Hg_{0.5}Bi_{0.5}Sr_2Pr_2Cu_2O_{9-\delta}$, respectively. For the "pure praseodymium" cuprates, EDS analysis reveals that the final composition of the phase is different from the nominal composition. One obtains an excess of alkaline with respect to the ideal formula leading to the compound $Hg_{0.4}Pr_{0.6}Sr_{2.3}Pr_{1.7}Cu_2O_{9-\delta}$; the substitution of barium for strontium allows more mercury to be introduced into the matrix, leading to the formula $Hg_{0.7}Pr_{0.3}Sr_{1.4}Ba_{0.8}Pr_{1.8}Cu_2O_{9-\delta}$.

The Perfect Structure

The XRD patterns of the different phases can be indexed in a tetragonal cell with $a \approx a_p$ and $c \approx 29.5$ Å; the refined parameters and compositions are given in Table 1. It can be seen that the cell volume is almost constant for the strontium cuprates (~441 Å^3) and significantly increased by the introduction of barium in agreement with the Sr and Ba radii (15). The electron diffraction analysis confirms the *I*-type symmetry of the cell, as illustrated by [001] and [100] ED patterns (Fig. 1). In the [001] pattern of Fig. 1a, one observes a fourfold arrangement of strong reflections at a reciprocal distance of 0.37 Å^{-1} from the origin; they correspond to the [110]-type reflections in the perovskite description. The ED pattern of the $Hg_{0.4}Sr_{2.3}Pr_{2.3}Cu_2O_{9-\delta}$ oxide, however, exhibits weak extra reflections with respect to the other patterns; this will be discussed below. HREM images have been obtained

TABLE 1

Composition	a (Å)	c (Å)	V (Å^3)
$(Hg_{0.4}Pr_{0.6})Sr_{2.3}Pr_{1.7}Cu_2O_9$	3.8603(2)	29.614(1)	441.30
$(Hg_{0.7}Pr_{0.3})Sr_{1.4}Ba_{0.8}Pr_{1.8}Cu_2O_9$	3.8914(8)	29.984(9)	453.95
$Hg_{0.3}Tl_{0.7}Sr_2Pr_2Cu_2O_9$	3.8642(1)	29.568(1)	441.36
$Hg_{0.3}Pb_{0.7}Sr_2Pr_2Cu_2O_9$	3.8631(2)	29.522(2)	440.57
$Hg_{0.5}Bi_{0.5}Sr_2Pr_2Cu_2O_9$	3.8657(2)	29.467(1)	440.34

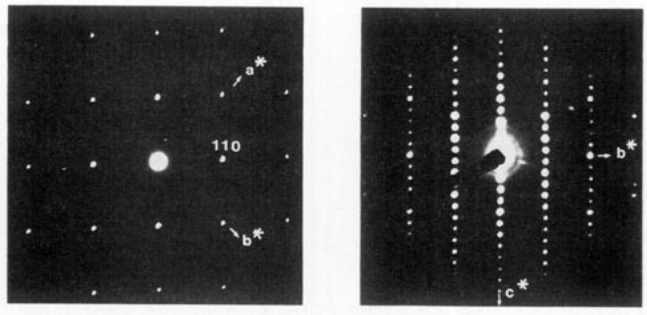

FIG. 1. (a) [001] and (b) [100] typical electron diffraction patterns of $[Hg_{1-x}M_x]Sr_2Pr_2Cu_2O_{9-\delta}$ cuprates.

along different sections; they confirm the 1222 crystal structure and allow one to deduce the sequence of the different cation layers. In the [100]-type images, one notes a regular sequence of layers: [SrO]–$[Hg_{1-x}M_xO_{1-\delta}]$–[SrO]–$[CuO_2]$–[Pr]–[Pr]–$[CuO_2]$. In the thinnest parts, all heavy ions are resolved, depending on the defocus value, as bright or dark dots. In Fig. 2, the unit cell has been outlined and the nature of the cations identified. The rows of copper appear as rows of gray dots, whereas Hg, Pr, and Sr appear as dark dots. This sequence leads to the schematic representation of the 1222 structure represented in Fig. 3.

In order to check this structural model, calculations have been performed from powder XRD data in the space group *I*4/*mmm* for the "Hg/Tl 1222" cuprate. The starting model is the one previously used for $Tl_{0.5}Pb_{0.5}Sr_2Gd_{2-x}Ce_xCu_2O_{9-\delta}$ (16); $SrHgO_2$ and HgO, detected as impurities, are introduced in the calculation as secondary phases. Positional parameters and isotropic thermal factors are refined successively except for the oxygen atoms

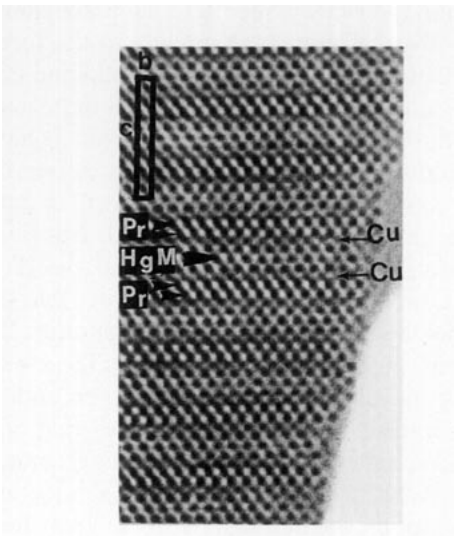

FIG. 2. [100] HREM image of the 1222 cuprate; the cell is outlined and the cations are imaged as dark dots.

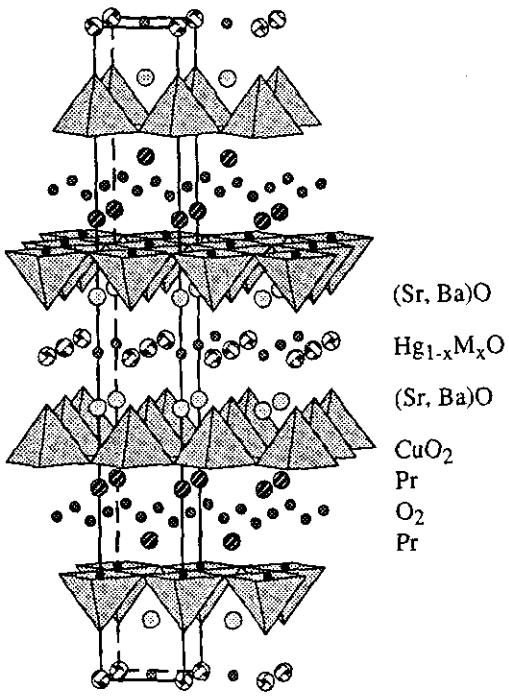

FIG. 3. Schematic representation of the 1222 crystal structure.

TABLE 2
Refined Variable Parameters for $Hg_{0.3}Tl_{0.7}Sr_2Pr_2Cu_2O_{9-\delta}$
[Space Group $I4/mmm$; a = 3.8642(1) Å, c = 29.568(1) Å]

Atom	Site	x/a	y/b	z/c	B (Å)^2
Hg/Tl	2*a*	0	0	0	2.2(2)
Sr	4*e*	0	0	0.5847(2)	0.0(2)
Pr	4*e*	0	0	0.7055(1)	1.1(2)
Cu	4*e*	0	0	0.1480(4)	0.912
O(1)	4*e*	0	0	0.068(1)	1.0[a]
O(2)	8*g*	0	½	0.1482(9)	1.0[a]
O(3)	4*d*	0	½	¼	1.0[a]
O(4)	2*b*	0	0	½	1.0[a]

Note. R_p = 10.1%, R_{wp} = 13.2%, χ^2 = 1.8, R_i = 9%.
[a] Value arbitrarily fixed.

whose B factors are fixed arbitrarily at 1 Å^2. After successive refinements, the different agreement factors are minimized for the parameters given in Table 2. Note that the low B value obtained for Sr suggests a partial occupancy of Sr sites by Pr and vice versa; this hypothesis cannot be tested due to the amounts of elements involved. The agreement between experimental and calculated XRD patterns is shown in Fig. 4. The interatomic M–O distances are given in Table 3. All these results attest to the "1222" nature of the structure of the studied compound.

In spite of the lack of accuracy in the M–O distances (Table 3) due to the low scattering factor of oxygen to X rays, some comments can be made concerning these distances:

(i) The apical (Hg/Tl)–O distance (d = 2.02 Å) is larger than that observed in pure mercury cuprates ($d \approx$ 1.95 Å) and is slightly smaller than that observed in pure monolayer thallium cuprates ($d \approx$ 2.04–2.06 Å),

(ii) The PrO_8 cages are elongated along the **c** direction; the O–O distances are 2.73 Å in the **ab** plane and 3.01 Å

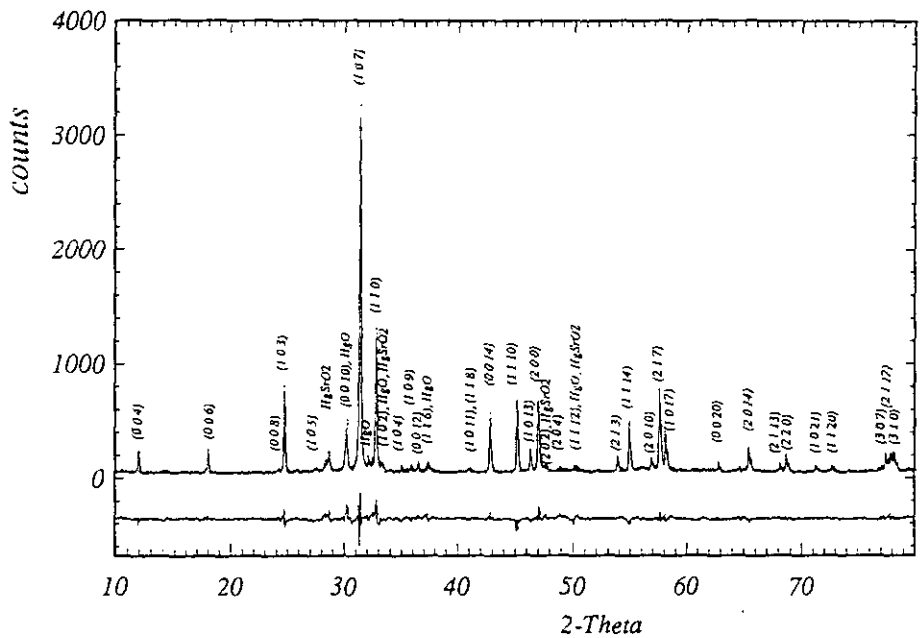

FIG. 4. Experimental and calculated XRD patterns of $[Hg_{1-x}M_x]Sr_2Pr_2Cu_2O_{9-\delta}$, M = Tl.

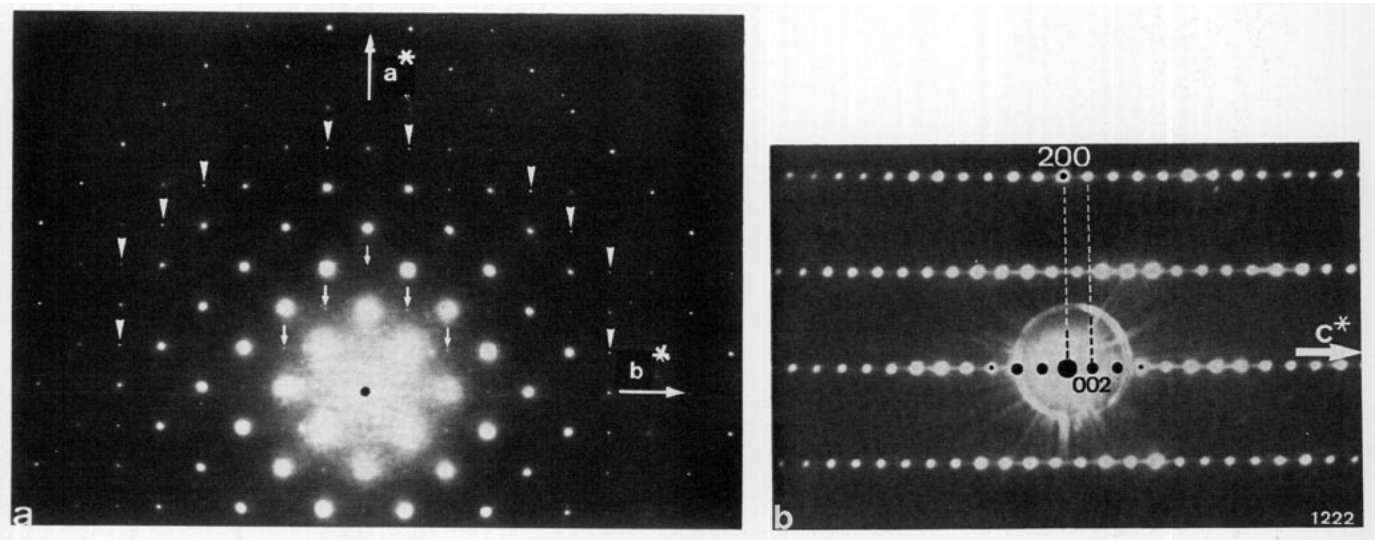

FIG. 5. Electron diffraction patterns of $Hg_{0.4}Sr_{2.3}Pr_{2.3}Cu_2O_{9-\delta}$; (a) along [001] with very weak 100 reflections, marked by small white arrows; (b) along [010], with streaking parallel to $\mathbf{c}^*$.

along **c**. This seems to be a common feature in cuprates involving double fluorite layers,

(iii) Praseodymium atoms are displaced from the center of the PrO_8 cages giving two sets of Pr–O distances (2.57 and 2.34 Å). This seems also to be a common feature of cuprates with double fluorite layers, e.g., distances of 2.67 and 2.32 Å, 2.68 and 2.33 Å are observed in Nd_2CuO_4 and Pr_2CuO_4, respectively (17); distances of 2.56 and 2.32 Å are observed in $Tl_{0.5}Pb_{0.5}Sr_2Gd_2Cu_2O_{9-\delta}$ (16). In each case the shortest distance involves oxygen atoms located at $z = \frac{1}{4}$, i.e., localized between the two Nd or Gd atoms.

(iv) The CuO_5 pyramids are characterized by four in-plane short distances (1.93 Å) and one long apical distance (2.36 Å).

Extended Defects in the $Hg_{0.4}Sr_{2.3}Pr_{2.3}Cu_2O_{9-\delta}$ Cuprate

A number of [001] ED patterns of this cuprate exhibit very weak 100 reflections, which should be absent in the *I4/mmm* space group (arrows, Fig. 5a). This phenomenon may be due to double diffraction from the first order Laue zone where the 101-type reflections are marked by arrowheads (Fig. 5a); however, they may also be reinforced due to the presence of (001)-type planar defects which cause streaking parallel to $\mathbf{c}^*$ (Fig. 5b); intensity at the 100-type position is indeed possible due to the intersection of diffuse streaks along $\mathbf{c}^*$ passing through the 101 reflections.

Several defects have been previously reported on the 1222-type structure (18). Three of them appear regularly in the cuprate $Hg_{0.4}Sr_{2.3}Pr_{2.3}Cu_2O_{9-\delta}$.

The first defect, shown in the center of Fig. 6, corresponds to the replacement of a single $[Hg_{1-x}Pr_xO_{1-\delta}]$ layer by a double $[Hg_{1-x}Pr_xO_{1-\delta}]_2$ layer introducing locally a 2222-type structure (Fig. 7). In Fig. 6 the configu-

TABLE 3
Selected Interatomic Distances (Å) for $Hg_{0.3}Tl_{0.7}Sr_2Pr_2Cu_2O_{9-\delta}$

Hg/Tl–O(1)	×2	2.02(3)	Pr–O(2)	×4	2.57(2)
Hg/Tl–O(4)	×4	2.732(1)	Pr–O(3)	×4	2.338(2)
Sr–O(1)	×4	2.775(5)	Cu–O(1)	×1	2.36(3)
Sr–O(2)	×4	2.69(2)	Cu–O(2)	×4	1.932(1)
Sr–O(4)	×1	2.504(6)			

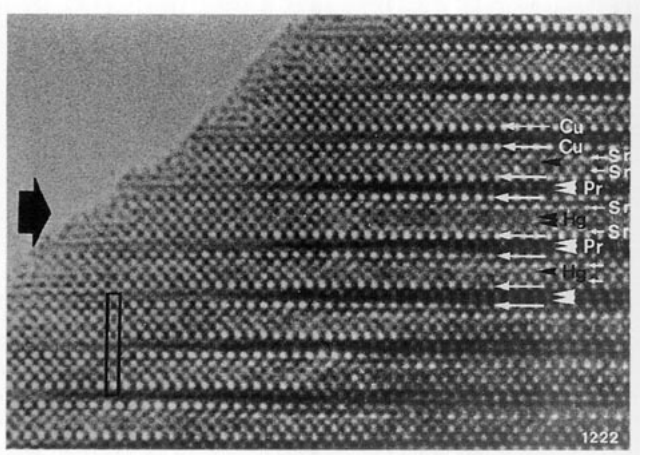

FIG. 6. [100] HREM image of $Hg_{0.4}Sr_{2.3}Pr_{2.3}Cu_2O_{9-\delta}$ where a single $[Hg_{1-x}Pr_x]O_{1-\delta}$ layer in replaced by a double $[Hg_{1-x}Pr_xO_{1-\delta}]_2$ layer, similar to the one observed in the 2212 and 2222 structures; the defect is indicated by the large black arrow.

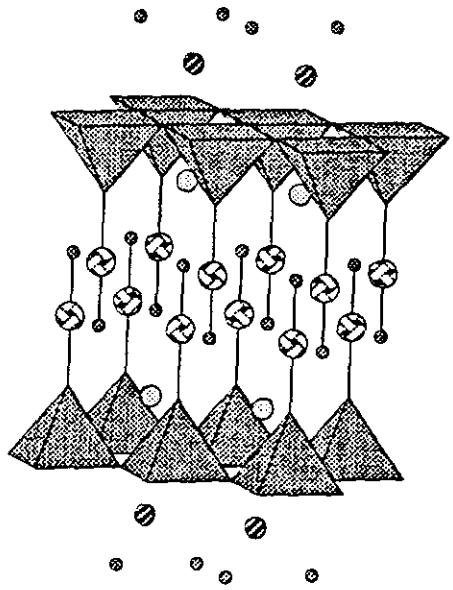

FIG. 7. Schematic representation in the double $[Hg_{1-x}Pr_xO_{1-\delta}]_2$ layer surrounded by two perovskite layers.

ration of the copper rows is accentuated: they appear as intense bright dots. Note that the "Hg–Pr"-2222 structure has been stabilized previously with barium for the cuprate $Hg_{1.5}Ba_2Pr_{2.3}Cu_{2.2}O_{10-\delta}$ (19).

A second type of defect is shown in Fig. 8a, imaged along [100] for similar defocus conditions as in Fig. 6. The Pr double layers are easily identified as the dark bands indicated by the double white arrowheads. A double Pr layer is locally eliminated; this leads to the formation of the "1201" structure (Fig. 8b) with the following sequence of layers: $[CuO_2]$–[SrO]–$[Hg_{1-x}Pr_xO_{1-\delta}]$–[SrO]–$[CuO_2]$–[SrO]–$[Hg_{1-x}Pr_xO_{1-\delta}]$–[SrO]. This phase exists in the Hg–Pr–Sr–Cu–O system, corresponding to the composition $(Hg_{0.4}Pr_{0.6})Sr_2CuO_{5-\delta}$ (20).

The third type of defect is shown in Fig. 9. Instead of having a double fluorite layer as in the perfect layer, we find here a slab of six layers in the fluorite configuration. Such defects have been previously treated in the Pb-1222 structure (21).

Order–Disorder Phenomena within the Mercury Layers

Detailed HREM observations of all these cuprates show that the cuprate $Hg_{0.4}Pr_{0.6}Sr_{2.3}Pr_{1.7}Cu_2O_{9-\delta}$ differs from the three other oxides, by an ordering of the cations in the $[Hg_{0.4}Pr_{0.6}O_{1-\delta}]_\infty$ layers. This feature is clearly observed on the [010] HREM images, especially in the areas with a crystal thickness between 100 and 200 Å (Fig. 10a). The double fluorite praseodymium layers are imaged as an almost continuous dark band and the $[(Hg, Pr)O_{1-\delta}]_\infty$ plane is characterized in contrast by dark dots corresponding to mercury that alternate with darker spots representing praseodymium (see arrows); thus the ordered sequence "Hg–Pr–Hg" leads to a doubling of the a parameter ($a \approx 2a_p \approx 7.6$ Å) (Fig. 10b). Such a phenomenon has previously been observed between mercury and praseodymium in the "1201" (20) and "1212" (13) cuprates. However, contrary to the latter cuprates, the "1222" phase $Hg_{0.4}Pr_{0.6}Sr_{2.3}Pr_{1.7}Cu_2O_{9-\delta}$ is not perfectly ordered. Within one "$Hg_{0.4}Pr_{0.6}$" layer the "$2a_p$" periodicity is often broken. Moreover, two successive "$Hg_{0.6}Pr_{0.6}$" layers are often randomly shifted with respect to each other, generating antiphase boundaries (18). In some places the 1–1 ordering is no longer visible, due to the inclination of the antiphase boundaries which produces mixed columns in projection.

These order–disorder phenomena are in fact responsible for the weak type reflections (Fig. 5a) and partly the streaks observed in the [010] ED patterns along **c**.

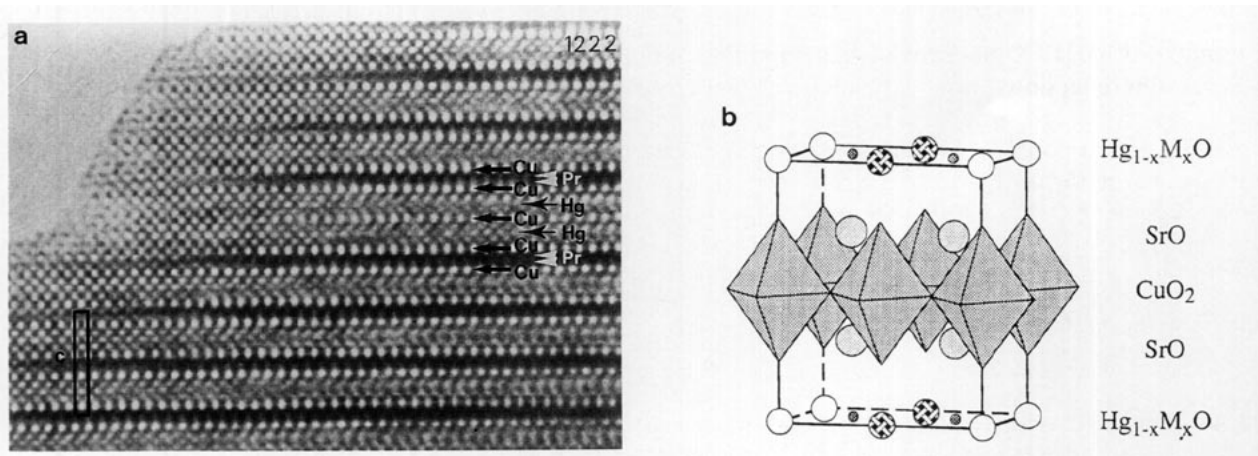

FIG. 8. (a) [100] HREM image of $Hg_{0.4}Sr_{2.3}Pr_{2.3}Cu_2O_{9-\delta}$ where a 1201 member, $Hg_{0.4}Pr_{0.6}Sr_2CuO_{5-\delta}$, is locally formed; (b) schematic representation of the 1201 structure where Hg and M = Pr atoms are ordered along **a**.

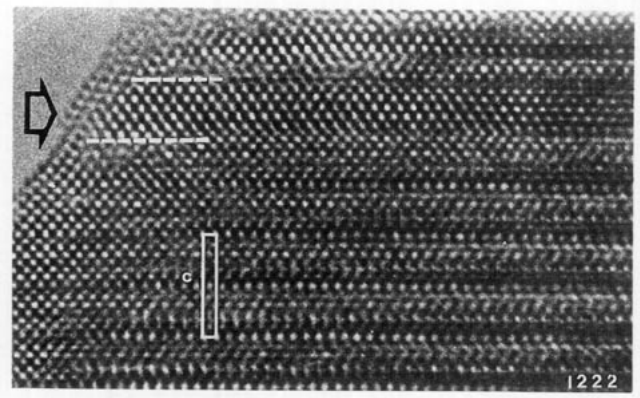

FIG. 9. [100] HREM image of $Hg_{0.4}Sr_{2.3}Pr_{2.3}Cu_2O_{9-\delta}$ where six adjacent fluorite-type layers are observed.

Contrary to the pure "Pr–Sr" cuprate, the Ba-substituted phase $(Hg_{0.7}Pr_{0.3})Sr_{1.4}Ba_{0.8}Pr_{1.8}Cu_2O_{9-\delta}$ does not exhibit any **c***-streaking; the HREM images (Fig. 11) show a diffuse variation of the contrast with randomly distributed more or less dark dots correlated to Pr and Hg atoms, respectively. This suggests an irregular distribution of the mercury and praseodymium atoms in the matrix similar to that observed in the Hg-rich 2212 (22) and 2222 (19).

The ability of the Tl(III), Pb(IV), and Bi(V) species to

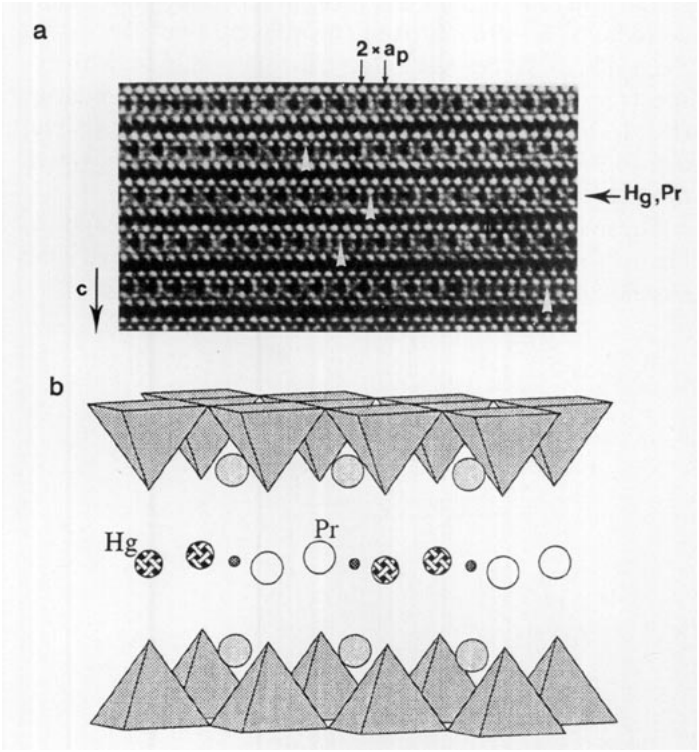

FIG. 10. [010] HREM image of $Hg_{0.4}Sr_{2.3}Pr_{2.3}Cu_2O_{9-\delta}$ where a doubling of the **a**-axis is observed, as a result of a Hg/Pr ordering. Praseodymium is imaged as the darker dots. It can be seen that the periodicity is often broken (see white arrowheads).

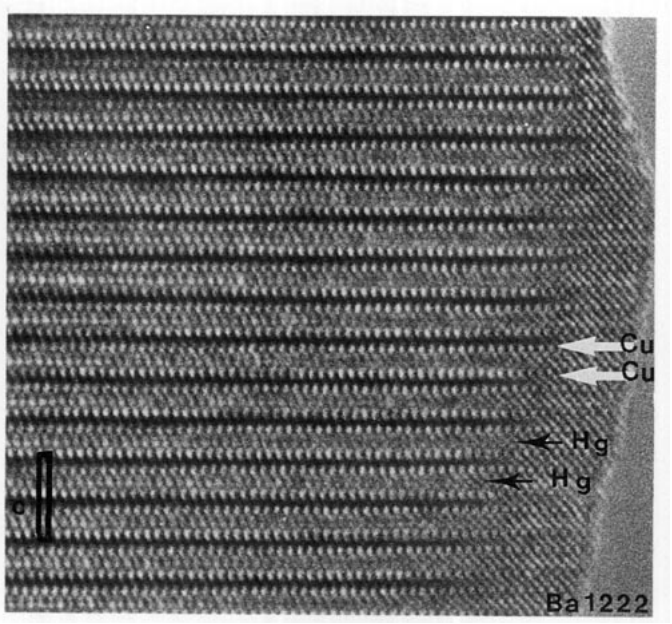

FIG. 11. [010] HREM image of $Hg_{0.7}Sr_{1.4}Ba_{0.8}Pr_{2.1}Cu_2O_{9-\delta}$ the Hg and Pr atoms are randomly distributed in the mixed layer.

be distributed statistically with Hg(II) within the rock-salt layers can be explained by their similar sizes and $5d^{10}$ electronic configurations. On the contrary, the presence of praseodymium in addition to mercury tends to induce an ordering, due to the different electronic configuration and size of these two species; nevertheless the ordering may be disturbed or destroyed by the introduction, in the adjacent layers, of larger cations such as barium, as previously observed for Ba–Hg "2222" and "2212" cuprates (19, 22).

Cleavage Phenomena

A remarkable characteristic of all these mercury "1222" cuprates deals with the easy cleavage of the crystals along the (001) plane between the "SrO" and one "$(Hg, M)O_{1-\delta}$" layer. This is illustrated in Fig. 12, where the $[CuO_2]_\infty$ layers are indicated by arrows. The top layer

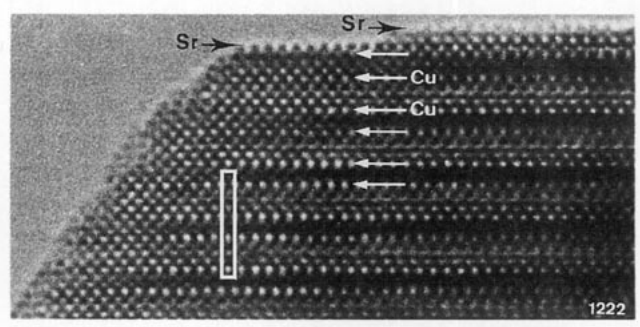

FIG. 12. [100] HREM image of $Hg_{0.4}Sr_{2.3}Pr_{2.3}Cu_2O_{9-\delta}$ illustrated that the cleavage of the crystals always involves [SrO] as the top layer.

is always a [SrO] layer as shown by the two black arrows that correspond to two different levels. This suggests that a mercury-based top layer is not a stable configuration. Note that this cleavage is different from that obtained between bismuth or thallium bilayers in the corresponding 2212 cuprates.

Transport Properties

The resistance and SQUID measurements do not allow superconductivity to be detected at temperatures down to 4.2 K. All samples are either semiconductors or insulators. This is illustrated for the oxide $Hg_{0.4}Pr_{0.6}Sr_{2.3}Pr_{1.7}Cu_2O_{9-\delta}$, that exhibits a semiconducting behavior in the range 150–280 K with an activation energy of 1.8 eV. Moreover, its conductivity cannot be improved by annealing in oxygen up to 100 bar, for 9 hr at 300°C. The oxide $Hg_{0.7}Pr_{0.3}Sr_{1.4}Ba_{0.8}Pr_{1.8}Cu_2O_{9-\delta}$ is an even worse conductor with a resistivity of 10^7 Ω cm at 300 K, to be compared with 10^2 Ω cm for $Hg_{0.4}Pr_{0.6}Sr_{2.3}Pr_{1.7}Cu_2O_{9-\delta}$ at the same temperature; its resistivity is too high to be measured with our method at room temperature. This suggests that the substitution of barium for strontium influences the hybridization of the copper–oxygen orbitals in agreement with the results previously obtained for the 1212-type cuprates $TlBa_{2-x}Sr_xLnCu_2O_7$ (23).

CONCLUSION

Five mercury-based cuprates with the "1222" structure have been synthesized for the first time. This confirms the great ability to accommodate foreign cations such as thallium, lead, and praseodymium in the intermediate layers $[Hg_{1-x}A_xO_{1-\delta}]_\infty$. The great flexibility of the structure also explains the presence of various extended defects to be accommodated, suggesting the possibility of generating new intergrowths. The absence of superconductivity in these phases reinforces our conviction that the presence of double fluorite layers is not favorable to the appearance of this property. One indeed observes that most of the cuprates involving double fluorite layers either do not superconduct or exhibit low diamagnetic volume fractions.

REFERENCES

1. B. Raveau, C. Michel, M. Hervieu, and D. Groult, "Crystal Chemistry of HTS Oxides," Springer Series in Material Science, Vol. 15, p. 207. Springer, Berlin, 1991.
2. B. Domengès, M. Hervieu, C. Martin, D. Bourgault, C. Michel, and B. Raveau, *Phase Transitions* **19,** 231 (1989).
3. C. Martin, D. Bourgault, M. Hervieu, C. Michel, J. Provost, and B. Raveau, *Mod. Phys. Lett. B* **3,** 993 (1989).
4. Y. Tokura, T. Arima, H. Takagi, S. Uchida, T. Ishigaki, K. Asano, R. Bayers, A. I. Nazzal, P. Lacorre, and J. B. Torrance, *Nature* **342,** 890 (1989).
5. T. Arima, Y. Tokura, H. Takagi, S. Uchida, R. Bayers, and J. B. Torrance, *Physica C* **168,** 79 (1990).
6. S. Adachi, O. Inone, S. Kawashima, H. Adachi, Y. Ichikawa, K. Setsune, and K. Wasa, *Physica C* **168,** 1 (1990).
7. T. Maeda, K. Sakuyama, S. Korigama, A. Ichinose, H. Yamanchi, and S. Tanaka, *Physica C* **169,** 133 (1990).
8. H. Sawa, S. Suzuki, M. Watanabe, J. Akimitsu, H. Matsubara, H. Watabe, S. Uchida, K. Kokusho, H. Asano, F. Izumi, and E. Takayama-Muromachi, *Nature* **337,** 347 (1989).
9. T. Mochiku, T. Nagashima, Y. Saito, M. Watahiki, H. Asuno, and Y. Fakai, *Jpn. J. Appl. Phys.* **29,** L588 (1990).
10. S. N. Putilin, E. V. Antipov, and M. Marezio, *Physica C* **212,** 266 (1993).
11. S. F. Hu, D. A. Jefferson, R. S. Liu, and P. P. Edwards, *J. Solid State Chem.* **103,** 280 (1993).
12. D. Pelloquin, M. Hervieu, C. Michel, G. Van Tendeloo, A. Maignan, and B. Raveau, *Physica C* **216,** 257 (1993).
13. M. Hervieu, G. Van Tendeloo, A. Maignan, C. Michel, F. Goutenoire, and B. Raveau, *Physica C* **216,** 264 (1993).
14. D. B. Wiles and R. A. Young, *J. Appl. Crystallogr.* **14,** 149 (1981).
15. R. D. Shannon, *Acta Crystallogr. Sect. A* **32,** 751 (1976).
16. R. Vijayaraghavan, C. Michel, A. Maignan, M. Hervieu, C. Martin, and B. Raveau, *Physica C* **206,** 81 (1993).
17. J. Gopalakrishan, M. A. Subramanian, C. C. Torardi, J. P. Attfield, and A. W. Sleight, *Mater. Res. Bull.* **24,** 321 (1989).
18. G. Van Tendeloo, M. Hervieu, X. F. Zhang, and B. Raveau, *J. Solid State Chem.*, to appear.
19. M. Huvé, C. Martin, A. Maignan, C. Michel, G. Van Tendeloo, M. Hervieu, and B. Raveau, *J. Solid State Chem.* **114,** 230 (1995).
20. F. Goutenoire, P. Daniel, M. Hervieu, G. Van Tendeloo, C. Michel, A. Maignan, and B. Raveau, *Physica C* **216,** 243 (1993).
21. M. T. Gambardella, B. Domengès, T. Rouillon, M. Hervieu and B. Raveau, *Eur. J. Solid State Inorg. Chem.* **29,** 333 (1992).
22. C. Martin, M. Hervieu, G. Van Tendeloo, F. Goutenoire, C. Michel, A. Maignan, and B. Raveau, *Solid State Commun.* to appear.
23. M. Huvé, C. Martin, C. Michel, A. Maignan, M. Hervieu, and B. Raveau, *J. Phys. Chem. Solids* **54,** 145 (1993).